Journal of Hazardous Materials 199–200 (2012) 301–308

Contents lists available at SciVerse ScienceDirect

Journal of Hazardous Materials

journal homepage: www.elsevier.com/locate/jhazmat

# Preparation, characterization and performance of a novel visible light responsive spherical activated carbon-supported and $Er^{3+}$:$YFeO_3$-doped $TiO_2$ photocatalyst

Dianxun Hou[a,b], Liang Feng[a,c], Jianbin Zhang[a], Shuangshi Dong[a,*], Dandan Zhou[a], Teik-Thye Lim[b]

[a] Key Lab of Groundwater Resources and Environment, Ministry of Education, Jilin University, Changchun 130021, China
[b] School of Civil and Environmental Engineering, Nanyang Technological University, 50 Nanyang Avenue, Singapore 639798, Republic of Singapore
[c] College of Environmental Science and Technology, Tongji University, Shanghai 200092, China

ARTICLE INFO

*Article history:*
Received 26 July 2011
Received in revised form 5 October 2011
Accepted 3 November 2011
Available online 9 November 2011

*Keywords:*
Upconversion luminescence agent
Visible light
Photocatalytic degradation
Calcination temperature
Catalyst regeneration

ABSTRACT

A novel spherical activated carbon (SAC) supported and $Er^{3+}$:$YFeO_3$-doped $TiO_2$ visible-light responsive photocatalyst ($Er^{3+}$:$YFeO_3$/$TiO_2$-SAC) was synthesized by a modified sol–gel method with ultrasonic dispersion. It was characterized by scanning electron microscope (SEM), energy dispersive X-ray spectroscope (EDS), powder X-ray diffractometer (XRD) and UV–vis diffuse reflectance spectrophotometer (DRS). The photocatalytic activity of $Er^{3+}$:$YFeO_3$/$TiO_2$-SAC was evaluated for degradation of methyl orange (MO) under visible light irradiation. The effects of calcination temperature and irradiation time on its photocatalytic activity were examined. The experimental results indicated that $Er^{3+}$:$YFeO_3$ could function as an upconversion luminescence agent, enabling photocatalytic degradation of MO by $TiO_2$ under visible light. The $Er^{3+}$:$YFeO_3$/$TiO_2$ calcinated at 700 °C showed the highest photocatalytic capability compared to those calcinated at other temperatures. The photocatalytic degradation of MO followed the Langmuir–Hinshelwood kinetic model. Although the photocatalyst showed a good physical stability and could tolerate a shear force up to $25 \times 10^{-3}$ N/g, its photocatalytic activity decreased over a four-cycle of reuse in concentrated MO solution, indicating that the decreased activity was ascribed to the fouling of catalyst surface by MO during the degradation process. However, the fouled $Er^{3+}$:$YFeO_3$/$TiO_2$-SAC could be regenerated through water rinsing-calcination or acid rinsing-calcination treatment.



## 1. Introduction

Effluents from textile industry were usually treated with biological or conventional physicochemical techniques before discharged into surface water bodies [1]. However, it was difficult to degrade the dye pollutants completely via these techniques. $TiO_2$ was firstly reported by Fujishima and Honda in 1972 to be able to generate various reactive oxygen species in water such as hydroxyl radicals, hydrogen peroxide, superoxide radical anions, etc., under UV irradiation [2]. Since then, $TiO_2$ has widely been investigated for photocatalytic degradation of organic dyes because of its strong photoactive ability, high stability, non-toxicity and low cost [3,4]. It is necessary to supply the photons with energy higher than the $TiO_2$ band gap energy ($E_g$) in order to initiate actinic reactions. For the two crystal structures of $TiO_2$, namely anatase ($E_g$ = 3.2 eV) and rutile ($E_g$ = 3.02 eV), their absorption thresholds correspond to 380 and 410 nm [4,5]. However, the solar energy of above 3.0 eV ($\lambda$ < 410 nm) is less than 5% [6]. Consequently, the solar light utilization efficiency of the virgin $TiO_2$ is less than 5%, which limits its commercial application. In order to extend the light-responsive region of the photocatalyst, previous researchers [7–10] have developed upconversion luminescence agents such as $Er^{3+}$:$YAlO_3$ and $Er^{3+}$:$Y_3Al_5O_{12}$ which can transform the visible light into UV, and thus enable photogeneration of $e^-/h^+$ in $TiO_2$. Iron dopant has been found as a promoter to photocatalysis, and the anatase $TiO_2$ doped with iron has shown a good performance for the photocatalytic reaction of Congo red [11] and methyl orange [12].

In order to recover the $TiO_2$ nanoparticles from the treated water, $TiO_2$ can be immobilized on various particulate supports [3]. Since activated carbon is a highly porous material with high affinity for various organic pollutants, it can promote mass transfer in the heterogeneous photocatalysis. Thus, $TiO_2$ supported on activated carbon could enhance photocatalytic degradation of various organic pollutants [13–16].

The underlying hypothesis of this study is that the compound $Er^{3+}$:$YFeO_3$ combining iron, erbium and yttrium could function as an upconversion luminescence for photoexciting $TiO_2$ under visible light. The $Er^{3+}$:$YFeO_3$-doped $TiO_2$ immobilized on the spherical activated carbon particles ($Er^{3+}$:$YFeO_3$/$TiO_2$-SAC) could be a novel photocatalyst that would exhibit a synergistic adsorption-photocatalytic degradation of organic pollutants under visible-light irradiation. The other advantage of the prepared photocatalyst

* Corresponding author. Tel.: +86 13604431853.
*E-mail address:* dongshuangshi@gmail.com (S. Dong).

0304-3894/$ – see front matter © 2011 Elsevier B.V. All rights reserved.
doi:10.1016/j.jhazmat.2011.11.011

is that it is much easier to recover for reuse or regeneration. In this study, the $Er^{3+}$:$YFeO_3$/$TiO_2$-SAC composite was prepared and methyl orange (MO) was used as the model pollutant for evaluation of its performance. The effect of calcination temperature on MO decomposition rate and the degradation kinetics, were investigated under visible light irradiation at room temperature. The physical stability of the composite photocatalyst and its reusability were also investigated.

## 2. Experimental and methods

### 2.1. Catalyst preparation

#### 2.1.1. Synthesis of $Er^{3+}$:$YFeO_3$

The synthesis method of $Er^{3+}$:$YFeO_3$ was based on the synthesis of $Er^{3+}$:$YAlO_3$ [8,9] and $YFeO_3$ [17]. Stoichiometric amounts of $Y(NO_3)_3{\cdot}6H_2O$ and $Er(NO_3)_3{\cdot}6H_2O$ were dissolved in the deionized water. Then, $Fe(NO_3)_3$ was mixed into the above solution under vigorous agitation for 1 h at room temperature. The molar ratio of Er:Y:Fe was controlled at 0.01:0.99:1.00. After that, certain molar solid citric acid was added (molar ratio of citric acid:metal ion of 3:1). The final solution was evaporated at 85 °C in a water bath until a tawny, translucent and viscous gel appeared, which was dried at 130 °C for 24 h followed by ultrasonic dispersion to obtain dry powders. The dry sample was calcinated at 800 °C in a muffle furnace for 2 h, followed by grinding and ultrasonic treatment, to obtain the nanocrystalline $Er^{3+}$:$YFeO_3$ powder.

#### 2.1.2. Preparation of $Er^{3+}$:$YFeO_3$/$TiO_2$-SAC

The $Er^{3+}$:$YFeO_3$/$TiO_2$-SAC was prepared through the sol–gel technique. Solution A, which comprised 106.33 ml $Ti(OC_4H_9)_4$ and 243.08 ml $C_2H_5OH$ (95%), was stirred for 30 min at room temperature. Solution B comprising 1.0 g $Er^{3+}$:$YFeO_3$, 17.90 ml $CH_3COOH$, 11.28 ml $H_2O$, and 121.54 ml $C_2H_5OH$ (95%) was mixed rigorously. 1 ml HCl (0.1 M) was added to the solution B for controlling its pH value at around 4.0. Afterwards, the solution B was added drop-wise into the solution A with vigorous stirring and ultrasonic dispersion. Then 50 g of spherical activated carbon (SAC) particles (0.6 mm in diameter, Kureha Corp, Japan) were added into the resultant mixture during ultrasonic treatment. After curing for 24 h, the particles coated with $Er^{3+}$:$YFeO_3$/$TiO_2$ were separated from the solution, rigorously rinsed with ethanol followed by deionized water, and dried at 130 °C for 2 h. The dry sample was then calcinated at various temperatures (400, 500, 600, 700 and 800 °C) in a muffle furnace for 2 h, with a heating rate of 5 °C/min. For comparison, $Er^{3+}$:$YFeO_3$/$TiO_2$ samples calcinated at similar temperatures were also prepared.

### 2.2. Photocatalytic degradation of MO

The photocatalytic activity of $Er^{3+}$:$YFeO_3$/$TiO_2$-SAC was evaluated by investigating MO degradation. 1.00 g of photocatalyst was added to 50 ml of 500 mg/L MO solution. The experiment was conducted at room temperature and the pH was maintained at its natural value of 5.9 throughout. The suspension was irradiated by a 18 W-LED lamp with aeration by air flow of 0.6 L/min to obtain a uniform concentration distribution within MO solution. Fig. 1 shows the emission spectrum of the LED, which indicates major peaks at 455.0 nm and 552.9 nm, while UV was not detected (with TN-2234UVC, TAINA, Taiwan). The MO concentration was determined by an UV–vis spectrophotometer at 464 nm. All the experiments were carried out in a dark chamber to avoid interference of ambient light on the photoreaction.

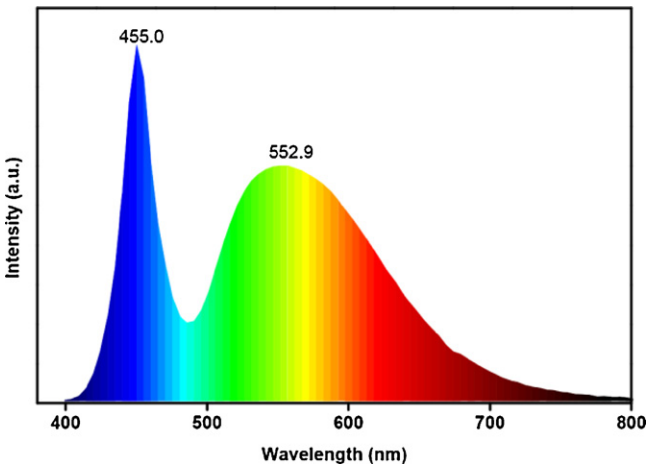


**Fig. 1.** Light spectrum of the LED lamp.

### 2.3. Durability and regeneration of photocatalyst

A series of experiments were conducted to evaluate the physical stability of $Er^{3+}$:$YFeO_3$/$TiO_2$-SAC and its ability for regeneration. In the physical stability experiment, 0.4, 1.0, 2.0 and 4.0 g of $Er^{3+}$:$YFeO_3$/$TiO_2$-SAC was added to varying amounts of the deionized water at a constant solid-to-liquid ratio of 1 g to 50 ml, into 100, 250, 500, 1000 ml beakers, respectively. Then the beakers were placed in a rotary shaker for 2 h at agitation speeds of 130 rpm and 180 rpm, respectively, to examine the effect of shear force on the physical stability of the composite photocatalyst. In addition, to evaluate the effects of shaking time, five of the same 500 ml beakers with 2.0 g photocatalyst and 100 ml deionized water, was placed on the rotary shaker for 1, 2, 3, 4 and 5 h at 130 rpm, respectively. The measurement method of the $TiO_2$ content in $Er^{3+}$:$YFeO_3$/$TiO_2$-SAC was estimated according to method adopted by Wang et al. [18].

To evaluate the photocatalytic life-time of $Er^{3+}$:$YFeO_3$/$TiO_2$-SAC, the used photocatalyst was recovered from the previous solution by a pipette, oven-dried at 105 °C, and then added to the next batch of fresh MO solution. The experiment was repeated up to four cycles. Another experiment was carried out to evaluate the regenerability of the $Er^{3+}$:$YFeO_3$/$TiO_2$-SAC. In this experiment, the recovered $Er^{3+}$:$YFeO_3$/$TiO_2$-SAC was treated with three different regeneration methods, namely, deionized water rinsing, deionized water rinsing-calcination (300 °C), acid rinsing (0.5 M HCl)-calcination (300 °C).

## 3. Results and discussion

### 3.1. Photocatalyst characterization

SEM and EDS analyses were performed by a scanning electron microscope (Quanta 200 ESEM, FEI, USA) in order to examine the morphology and elemental contents of the samples. The SEM image of the $Er^{3+}$:$YFeO_3$/$TiO_2$ (Fig. 2a) reveals the bulk form of the $Er^{3+}$:$YFeO_3$/$TiO_2$ with particle sizes of 200–400 nm. Fig. 2b shows the distribution of $Er^{3+}$:$YFeO_3$/$TiO_2$ (calcinated at 700 °C) on the surface of SAC. It appeared that $Er^{3+}$:$YFeO_3$/$TiO_2$ was not washed off by the ultrasonic treatment, which indicated a strong attachment of the $Er^{3+}$:$YFeO_3$/$TiO_2$ particles onto SAC. Fig. 3 shows the EDS spectra corresponding to the two points (points A and B) in Fig. 2b as well as the spectra for the virgin SAC and the $Er^{3+}$:$YFeO_3$/$TiO_2$. Compared with the EDS of the virgin SAC (Fig. 3a), the presence of additional peaks associated with Er, Y, Fe, and Ti indicated the successful syntheses of $Er^{3+}$:$YFeO_3$/$TiO_2$ and $Er^{3+}$:$YFeO_3$/$TiO_2$-SAC (Fig. 3b–d). Table 1 indicates that there was only a slight difference

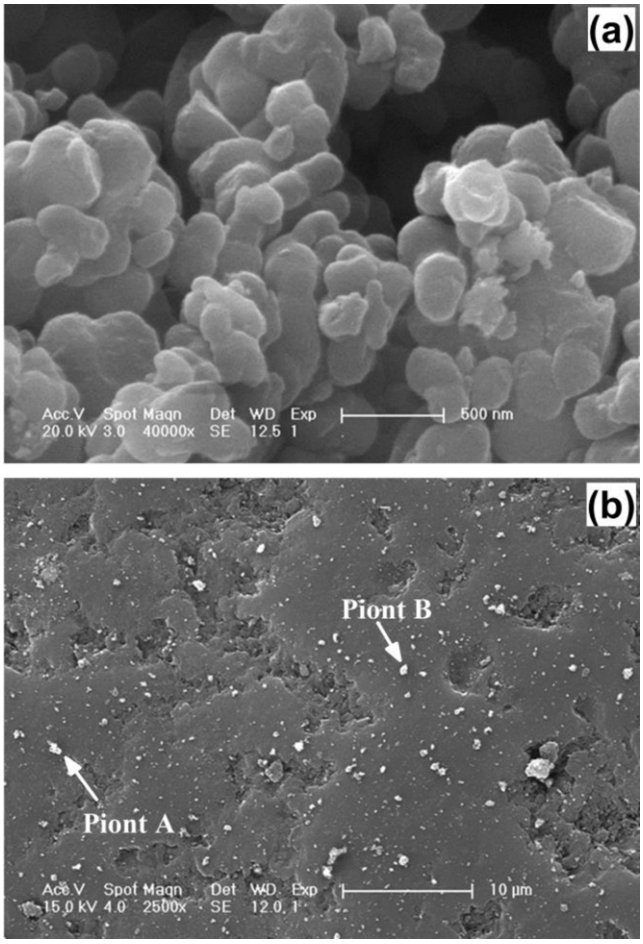


**Fig. 2.** SEM images of (a) $Er^{3+}$:$YFeO_3$/$TiO_2$ and (b) $Er^{3+}$:$YFeO_3$/$TiO_2$-SAC which were calcinated at 700 °C.

**Table 1**
Elemental contents on $Er^{3+}$:$YFeO_3$/$TiO_2$-SAC surface.

| Elements | Point | |
|---|---|---|
| | A (wt%) | B (wt%) |
| Y | 1.21 | 1.47 |
| Ti | 36.55 | 21.66 |
| Fe | 1.03 | 2.78 |
| Er | 1.79 | 1.28 |

in the elemental contents at point A and point B of Fig. 2b for the $Er^{3+}$:$YFeO_3$/$TiO_2$-SAC sample.

The crystal phases of the samples were confirmed by powder X-ray diffractometer (RINT 2500, Rigaku Corporation, Japan) using Ni filtered Cu K$\alpha$ radiation in the range of 2$\theta$ from 10° to 90°. Fig. 4a shows the XRD pattern of 1.0 mol% $Er^{3+}$-doped $YFeO_3$ prepared through the sol–gel route and calcinated at 800 °C. The pattern possesses similar spectrum to that of the JCPDS data of $YFeO_3$, which indicated that $YFeO_3$-based crystal was formed. Fig. 4b presents the XRD patterns of $Er^{3+}$:$YFeO_3$/$TiO_2$ calcinated at various temperatures, in comparison with that of a commercial pure $TiO_2$ (Beijing Chemical Works). All $Er^{3+}$:$YFeO_3$/$TiO_2$ samples, except the one calcinated at 800 °C, showed the strong peak at 25.4°, which belongs to anatase $TiO_2$. The XRD pattern of $Er^{3+}$:$YFeO_3$/$TiO_2$ calcinated at 700 °C showed the highest peaks at 25.4° with a low peak at 27.4°, indicating the dominance of anatase phase over rutile phase. As the calcination temperature increased to 800 °C, a stronger peak at 2$\theta$ = 27.4° appears while the peak at 25.4° becomes much weaker (Fig. 4b), implying the transformation of anatase to rutile phase at this temperature.

The weight percent of anatase/rutile phase ratio could be determined by Spurr–Myers equation [19]. In addition, the mean size of a single crystallite can be estimated from full-width at half-maxima (FWHM) of XRD peak by using Scherrer's equation [20],

$$D = \frac{K\lambda}{\beta \cos\theta} \quad (1)$$

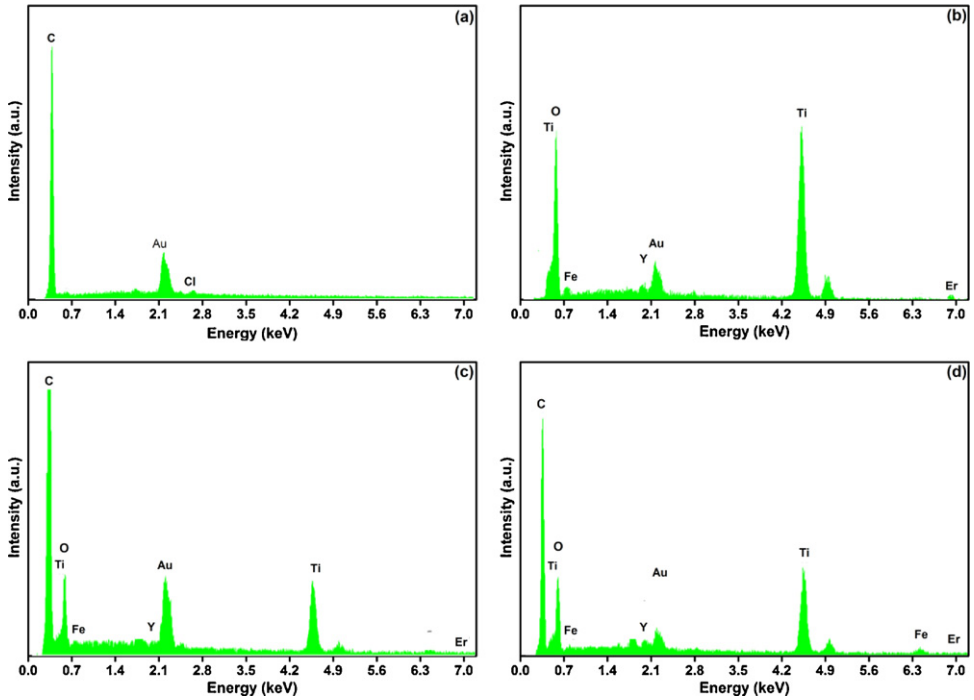


**Fig. 3.** EDS patterns of (a) SAC, (b) $Er^{3+}$:$YFeO_3$/$TiO_2$ calcinated at 700 °C, (c) point A and (d) point B in $Er^{3+}$:$YFeO_3$/$TiO_2$-SAC calcinated at 700 °C (Fig. 2b).

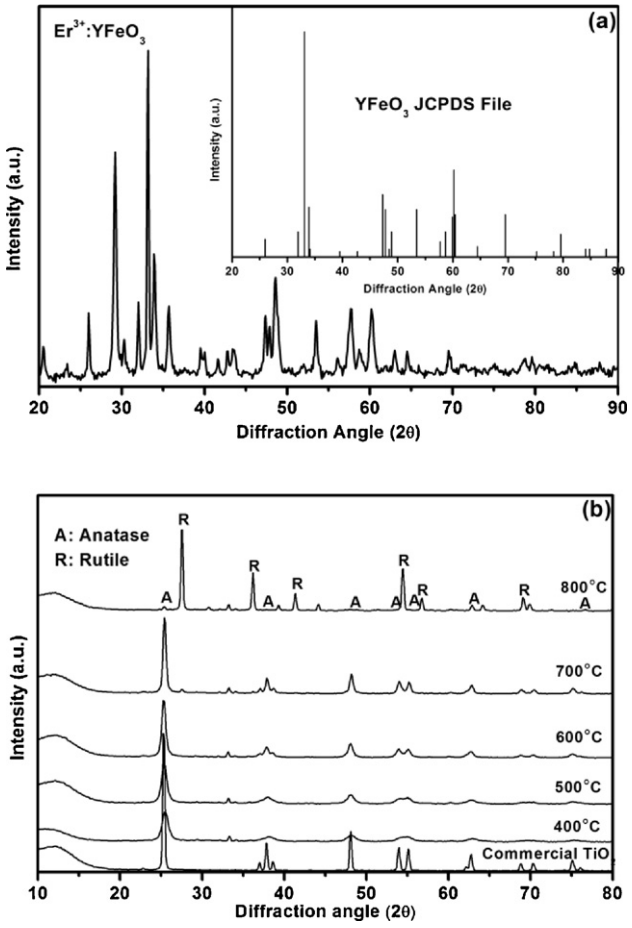


**Fig. 4.** XRD patterns of (a) $Er^{3+}$:$YFeO_3$ and (b) $Er^{3+}$:$YFeO_3/TiO_2$ calcinated at different temperatures as compared to the commercial $TiO_2$.

where $\lambda$ is the wavelength of the X-ray radiation (0.154 nm), $K$ is the Scherrer constant (0.9), $\theta$ is the Bragg angle (12.7°) and $\beta$ is the FWHM of the diffraction line broadening. The average sizes of the crystallites of the commercial $TiO_2$ powder and the synthesized catalysts calcinated at different temperatures are listed in Table 2. The results show that the crystal size of the commercial $TiO_2$ was larger than those loaded on the synthesized composite photocatalysts. The crystal size of $TiO_2$ in the composites increased with increasing calcination temperature suggesting that the high temperature treatment led to $TiO_2$ crystal growth, while the transformation of crystal phase occurred at calcination temperatures of 700 °C or higher.

Fig. 5 compares the absorption spectra for $Er^{3+}$:$YFeO_3$, commercial $TiO_2$, and the pure $Er^{3+}$:$YFeO_3/TiO_2$ (calcinated at various temperatures) measured with a UV–vis diffuse reflectance spectrophotometer (UV-3600, Shimadzu) using $BaSO_4$ as the reference.

**Table 2**
Average crystallite sizes and ratio of anatase-rutile in the photocatalyst samples.

| Photocatalyst | Crystallite size (nm) | Crystalline phase | |
|---|---|---|---|
| | | % Anatase | % Rutile |
| Commercial $TiO_2$ | 32.2 | 94.53 | 5.47 |
| $Er^{3+}$:$YFeO_3$ | 14.5 | – | – |
| $Er^{3+}$:$YFeO_3/TiO_2$-SAC 400 °C | 13.5 | 100 | 0 |
| $Er^{3+}$:$YFeO_3/TiO_2$-SAC 500 °C | 16.0 | 100 | 0 |
| $Er^{3+}$:$YFeO_3/TiO_2$-SAC 600 °C | 18.2 | 100 | 0 |
| $Er^{3+}$:$YFeO_3/TiO_2$-SAC 700 °C | 20.7 | 91.02 | 8.98 |
| $Er^{3+}$:$YFeO_3/TiO_2$-SAC 800 °C | 28.6 | 3.69 | 96.31 |

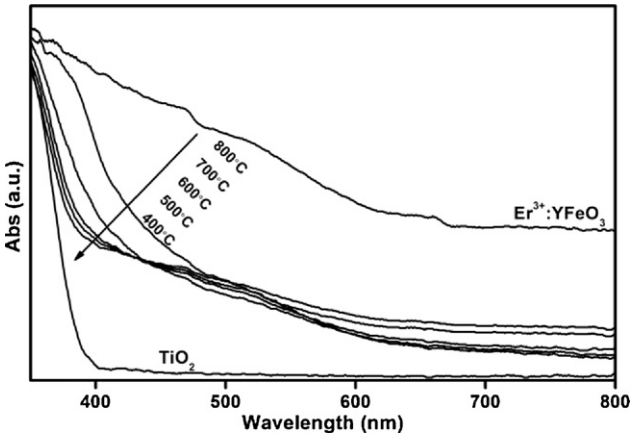


**Fig. 5.** UV–vis DRS spectra of $Er^{3+}$:$YFeO_3/TiO_2$ calcinated at different temperatures as compared to those of commercial $TiO_2$ and $Er^{3+}$:$YFeO_3$.

For this analysis, the $Er^{3+}$:$YFeO_3/TiO_2$/SAC was not analyzed because the sample with SAC support would absorb all the UV–vis light and not showing any absorption edge [21]. From the figure, the characteristic absorption edge for $Er^{3+}$:$YFeO_3$ is apparent at about $\lambda$ = 640 nm, indicating the potential upconversion luminescence activity. The characteristic absorption edges for $Er^{3+}$:$YFeO_3/TiO_2$ calcinated at various temperatures were around 600 nm, compared to that for the pure $TiO_2$ (at around 400 nm), which indicated that $Er^{3+}$:$YFeO_3/TiO_2$ still possessed the ability of visible light absorption. The difference in the spectral patterns should be ascribed to the difference in the crystallinity and crystal phase ratio presented in the samples (as reflected in Table 2). The rutile phase showed a higher light absorption than anatase phase in the visible light range of 400–500 nm.

### 3.2. Effect of calcination temperature

Fig. 6a shows a comparison between MO adsorption and MO photocatalytic degradation by $Er^{3+}$:$YFeO_3/TiO_2$-SAC with and without visible light irradiation. Without the visible light irradiation, the reduction of MO could be only attributed to its adsorption by SAC and the removal efficiency was around 36% in 80 min. When the $Er^{3+}$:$YFeO_3/TiO_2$-SAC calcinated at 400 °C, 500 °C, 600 °C, 700 °C and 800 °C were irradiated by the LED, the MO reduction percentages after 80 min reached 47.6%, 70.6%, 87.9%, 92.0% and 91.2%, respectively. It was evident that when the photocatalysts were irradiated by the visible light, the decreasing rates of MO concentration were much higher than that without visible light irradiation, indicating that MO was rapidly decomposed by the irradiated $Er^{3+}$:$YFeO_3/TiO_2$-SAC photocatalytically. In addition, the adsorption rate of MO on $Er^{3+}$:$YFeO_3/TiO_2$-SAC was much lower than that with the pure SAC, since some pores of the SAC in the former were blocked by the catalysts.

Fig. 6b shows the effect of calcination temperature on photocatalytic activity of $Er^{3+}$:$YFeO_3/TiO_2$-SAC for the degradation of MO under visible light irradiation. Apparently, the photocatalytic activity of $Er^{3+}$:$YFeO_3/TiO_2$-SAC could be enhanced with increasing calcination temperature from 400 °C to 700 °C. The MO degradation was the most rapid with the composite photocatalyst calcinated at 700 °C. However, the calcination temperature at 800 °C appeared to result in a slight decrease in the photocatalytic activity of the composite. The calcination at lower temperature (lower than 500 °C) led to a lower crystallinity of anatase $TiO_2$ phase and the $Er^{3+}$:$YFeO_3/TiO_2$ was not well formed, which resulted in a lower photocatalytic activity of the $Er^{3+}$:$YFeO_3/TiO_2$-SAC. Generally, anatase is more photoactive than rutile [22], since anatase is

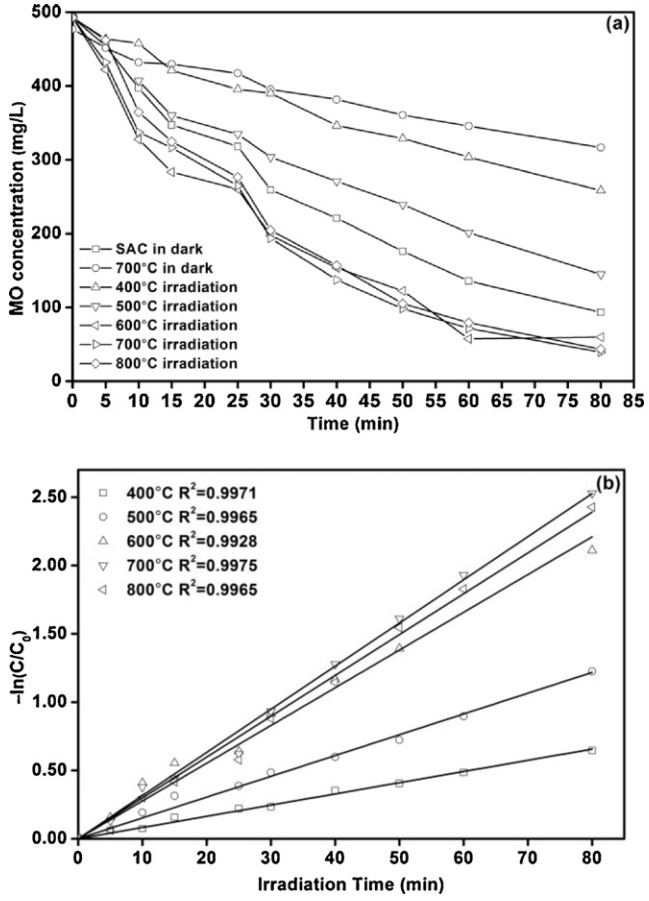


**Fig. 6.** (a) Decreases in MO concentration as a function of time by SAC and $Er^{3+}$:$YFeO_3$/$TiO_2$-SAC calcinated at different temperatures, (b) linear plots of the reaction kinetics for $Er^{3+}$:$YFeO_3$/$TiO_2$-SAC.

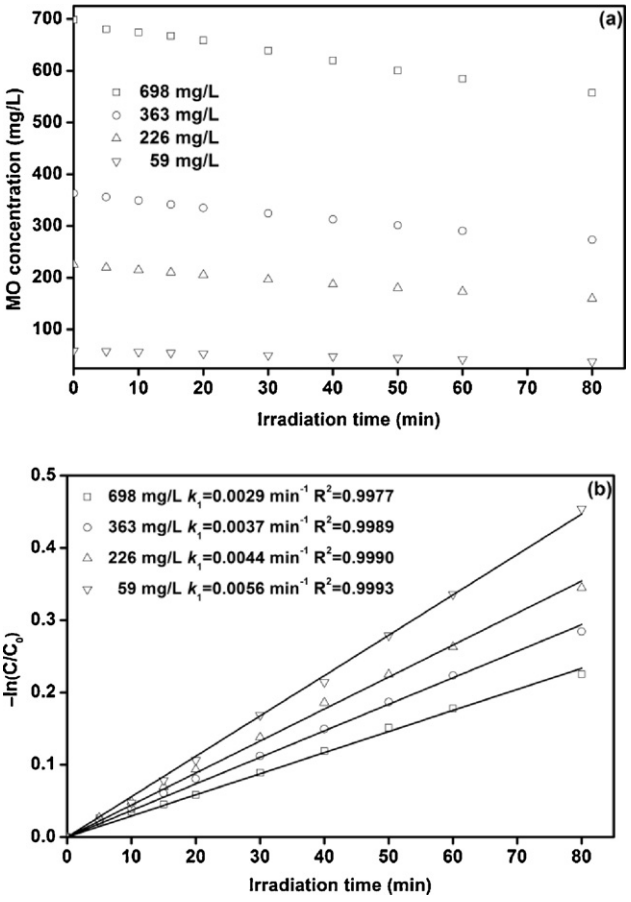


**Fig. 7.** (a) Effect of initial MO concentration on MO removal efficiency after adsorption equilibrium by $Er^{3+}$:$YFeO_3$/$TiO_2$-SAC calcinated at 700 °C, (b) linear plots of the reaction kinetics.

able to substantially ionosorb oxygen species, which are principally involved in electron capture in the aqueous phase reactions. Thus, it was predicted that that $Er^{3+}$:$YFeO_3$/$TiO_2$-SAC calcinated at 600 °C should possess the highest photocatalytic capability. However, the experimental finding was that $Er^{3+}$:$YFeO_3$/$TiO_2$-SAC with 700 °C heat-treatment appeared to be more photocatalytic under the visible light irradiation. The possible explanation is that the sample calcinated at 700 °C contained both anatase and rutile. As reported by Bickley et al. [23], for $TiO_2$ particle having an anatase core and a thin outlayer of rutile, the holes photogenerated by anatase core can be efficiently transferred to the rutile layer, thus enhancing photonic efficiency of the mixed $TiO_2$ phase. However, when the calcination temperature was raised to 800 °C, excessive dominance of rutile $TiO_2$ formed would reduce the photocatalytic activity of $Er^{3+}$:$YFeO_3$/$TiO_2$-SAC composite.

### 3.3. Effect of MO initial concentration and reaction kinetics

Four initial MO concentrations of 59, 226, 363 and 698 mg/L, achieved after 24 h of MO adsorption in dark, were evaluated for the effect of its initial concentration on its removal kinetics by $Er^{3+}$:$YFeO_3$/$TiO_2$-SAC calcinated at 700 °C. Fig. 7a shows continual decreases in MO concentrations with irradiation time from its initial concentrations, while Fig. 7b shows the linear plot of the corresponding photocatalytic degradation kinetics. In general, the MO degradation followed the pseudo-first-order kinetics for each of the given initial concentrations:

$$-\frac{dC}{dt} = k_1 C \tag{2}$$

where $k_1$ is the apparent pseudo-first-order reaction rate constant and $C$ is the MO concentration. The derived $k_1$ values corresponding to their respective initial MO concentrations are indicated in Fig. 7b. To analyze the influence of initial MO concentration on the reaction rate, Langmuir–Hinshelwood model is adopted:

$$\frac{1}{r_0} = \frac{1}{\kappa K'}\frac{1}{C_0} + \frac{1}{\kappa} \tag{3}$$

where $r_0$ is the initial reaction rate (mg/L min), $\kappa$ the Langmuir–Hinshelwood reaction rate constant (mg/L min), and $K'$ the Langmuir adsorption constant (L/mg). Fig. 8 shows the linear plot of $1/r_0$ versus $1/C_0$ and the derived values of Langmuir–Hinshelwood reaction rate constant and Langmuir adsorption constant.

### 3.4. Durability and regeneration of composite catalyst

#### 3.4.1. Effect of hydraulic conditions on the physical stability of $Er^{3+}$:$YFeO_3$/$TiO_2$-SAC

In the experiment investigating the physical stability of $Er^{3+}$:$YFeO_3$/$TiO_2$-SAC in suspension, the shear force (in N/g particle) exerted on $Er^{3+}$:$YFeO_3$/$TiO_2$-SAC particles was calculated according to the Chern's model [24] and the Ergun equations [25] (as detailed in Appendix A). The relationship between the remaining $TiO_2$ loading on $Er^{3+}$:$YFeO_3$/$TiO_2$-SAC and the applied shear force is plotted in Fig. 9a. The $TiO_2$ loading decreased marginally from 1.81 mg/g to 1.67 mg/g when the shear force was increased to $25 \times 10^{-3}$ N/g. When the shear force was increased further to $48 \times 10^{-3}$ N/g, $TiO_2$ loading decreased more drastically. Fig. 9b

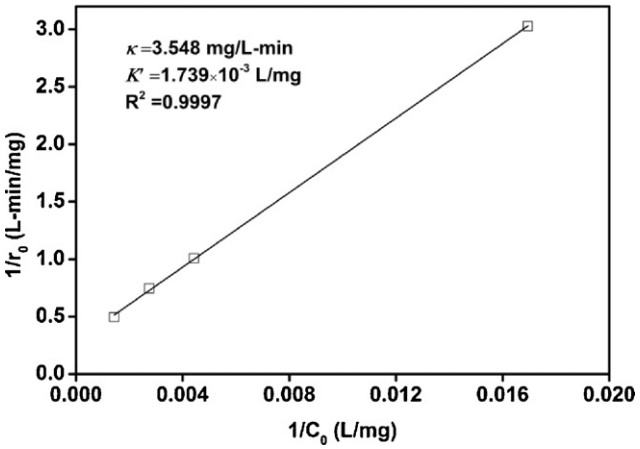


**Fig. 8.** Linear plot of $1/r_0$ versus $1/C_0$ based on Langmuir–Hinshelwood kinetic model.

shows the remaining $TiO_2$ loading on $Er^{3+}$:$YFeO_3$/$TiO_2$-SAC as a function of stirring time, when the shear force was maintained at $25 \times 10^{-3}$ N/g. It was evident that, in the first 4 h, the $TiO_2$ loading on $Er^{3+}$:$YFeO_3$/$TiO_2$-SAC decreased from 1.81 mg/g to 1.44 mg/g, which was equivalent to 20.0% reduction. However, in the fifth hour, the $TiO_2$ loading declined more significantly, corresponding to 32.6% reduction. Therefore, to maintain a robust physical stability of the $Er^{3+}$:$YFeO_3$/$TiO_2$-SAC composite for its practical application in suspension form, prolonged continual application in a single cycle or excessive hydrodynamic mixing should be avoided.

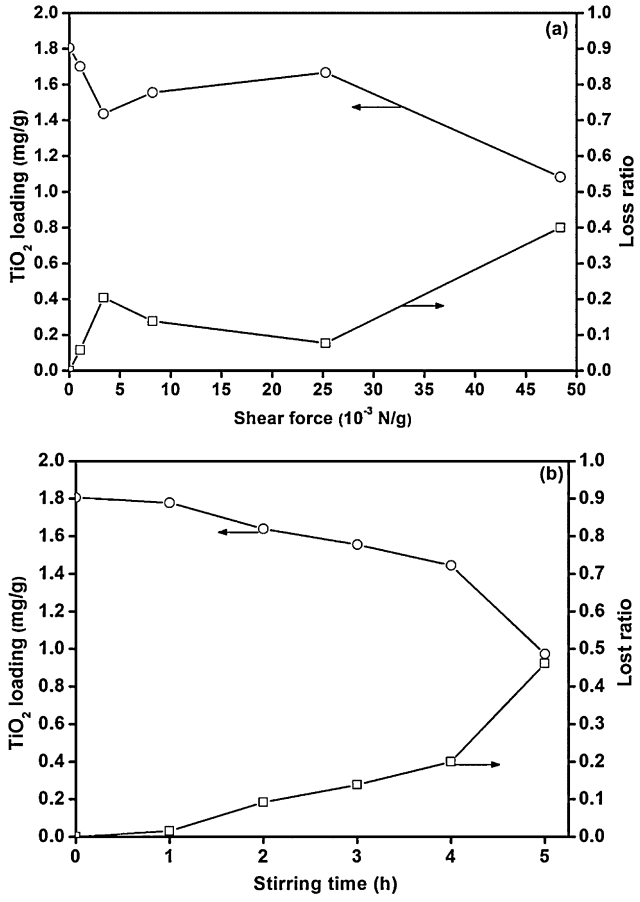


**Fig. 9.** Effects of (a) shear force on the $TiO_2$ loading on $Er^{3+}$:$YFeO_3$/$TiO_2$-SAC with a stirring time of 2 h, (b) stirring time on the $TiO_2$ loading on $Er^{3+}$:$YFeO_3$/$TiO_2$-SAC when shear force was maintained at $25 \times 10^{-3}$ N/g.

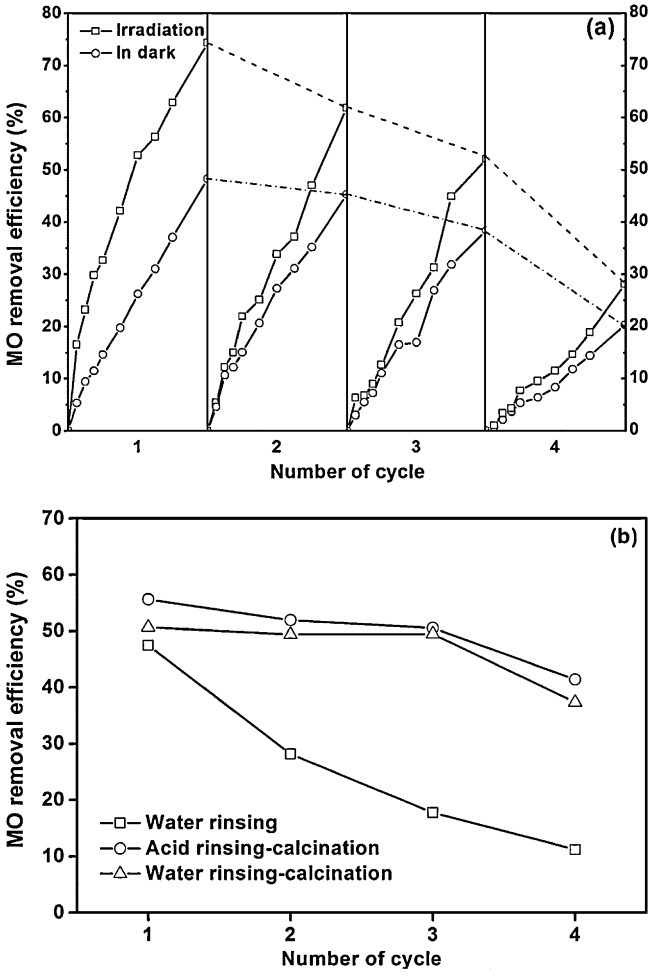


**Fig. 10.** (a) The effect of recycle time on the photocatalytic activity of $Er^{3+}$:$YFeO_3$/$TiO_2$-SAC calcinated at 700 °C, (b) photocatalyst regeneration (80 min in each cycle).

### 3.4.2. *Reusability of $Er^{3+}$:$YFeO_3$/$TiO_2$-SAC and regeneration*

Reuse of photocatalyst is very important in practical context. In order to evaluate the reusability of $Er^{3+}$:$YFeO_3$/$TiO_2$-SAC, the recycling of the composite catalyst for MO degradation was carried out. The results are shown in Fig. 10a. In the first cycle of 80 min under visible light irradiation, 74.3% MO was removed by the composite. After four cycles of use, the MO removal efficiency by the composite decreased to 28.1%. For comparison, a four-cycle removal of MO from solution in dark was performed, and the MO removal efficiency was found to decrease from 48.3% to 20.3% (Fig. 10a). The decrease of photocatalytic MO removal efficiency with increasing number of reuse could be attributed to the following reasons: (1) with the increase of number of use, MO accumulation on SAC could reduce its adsorption capacity, which to some extent, decreased its promotional effect on MO photocatalytic degradation; and (2) photocatalyst deactivation or fouling by the deposited MO molecules or its degradation by-products.

To evaluate possibility of regenerating the deactivated or fouled $Er^{3+}$:$YFeO_3$/$TiO_2$-SAC composite, water rinsing, water rinsing-calcination and acid rinsing-calcination treatments were adopted for regenerating the used composite. The acid rinsing was performed by mixing with 0.5 M HCl solution at a solid-to-liquid ratio of 1 g to 50 ml. During water rinsing and acid rinsing, the shear force was controlled at $25 \times 10^{-3}$ N/g for 30 min, in order to avoid loss of photocatalyst deposited on SAC. The calcination treatment was performed at 300 °C for 2 h.

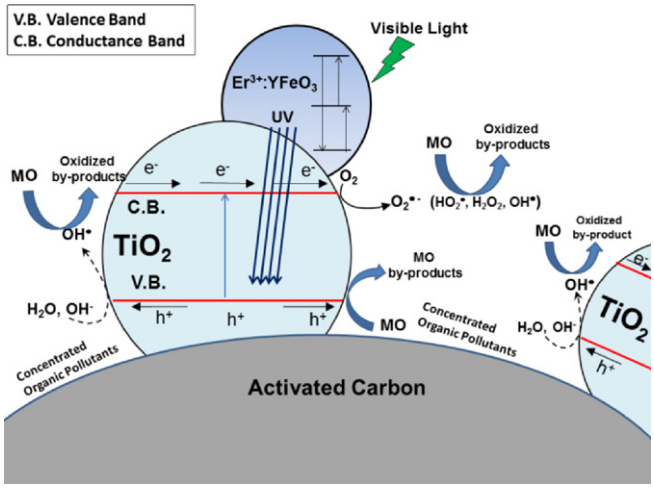


**Fig. 11.** Proposed mechanism for MO adsorption and degradation by the $Er^{3+}$:$YFeO_3$/$TiO_2$-SAC under visible light irradiation.

As shown in Fig. 10b, the water rinsing treatment appeared to exhibit similar decreasing trend of MO removal with respect to number of use without regeneration (Fig. 10a), indicating that a simple water rinsing could not regenerate the $Er^{3+}$:$YFeO_3$/$TiO_2$-SAC. On the other hand, the regeneration techniques of water rinsing-calcination and acid rinsing-calcination could almost completely regenerate the photocatalyst, whereby the photocatalytic MO removal efficiencies only decreased slightly from 52% to 50% and 56% to 50%, respectively, over the first three cycles (Fig. 10b). With these two techniques of regeneration, the regenerated $Er^{3+}$:$YFeO_3$/$TiO_2$-SAC was not found to be inactive at the fourth cycle of reuse. This implied that the loss of photocatalytic activity could be primarily attributed to the accumulation of MO and its by-products on the photocatalyst rather than the photocatalyst poisoning, and the photocatalytic activity could be effectively recovered by calcination.

### 3.5. *Proposed mechanism for MO degradation by $Er^{3+}$:$YFeO_3$/$TiO_2$-SAC*

Fig. 11 shows the possible mechanism for MO degradation by $Er^{3+}$:$YFeO_3$/$TiO_2$-SAC under visible light irradiation. The respective roles of SAC, $Er^{3+}$:$YFeO_3$ and $TiO_2$ are illustrated. In general, the photocatalytic reaction could proceed via two major steps:

(1) The activated carbon support is a highly porous material with a high affinity for various organic pollutants including dyes. It was able to adsorb MO from the suspension and promote its mass transfer to the surface of the SAC-supported $TiO_2$ whereby various reactive oxidizing species were produced, resulting in the enhanced photocatalytic degradation of MO [13–15].
(2) The upconversion luminescence agent ($Er^{3+}$:$YFeO_3$) at first absorbs the incident pump visible light and then continuously emits ultraviolet (UV), as shown in Fig. 11. The UV can effectively excite the $TiO_2$ nanoparticles and result in the formation of photo-generated electron–hole pairs [7–10]. The highly oxidative holes on valence band not only could directly decompose MO, but also oxidize $H_2O$ or $OH^-$ to form hydroxyl radicals ($OH^\bullet$). In addition, the photo-generated electrons at conduction band could be accepted by the dissolved oxygen in water, triggering a successive one-electron reductions of $O_2$ to form $O_2^{\bullet-}$, $HO_2^\bullet$, $H_2O_2$, and $OH^\bullet$. These radicals or reactive oxygen species are highly reactive with the surrounding organic pollutants (e.g., MO), leading to formation of degradation by-products and mineral acids or complete mineralization into $CO_2$ and $H_2O$.

## 4. Conclusion

In this study, $Er^{3+}$:$YFeO_3$/$TiO_2$-SAC, a novel activated carbon-supported visible-light responsive photocatalyst, was prepared by means of a modified ultrasonic dispersion and sol–gel method. The composite photocatalyst calcinated at 700 °C, in which the $TiO_2$ predominantly existed as anatase along with a small fraction of rutile, exhibited the highest photocatalytic activity under the white LED irradiation. In the composite photocatalyst, the $Er^{3+}$:$YFeO_3$ functioned as an upconversion luminescence agent to convert visible light into UV for photoexcitation of the $TiO_2$, while the activated carbon functioned as pollutant-concentrating photocatalyst support. This dual-functionality could synergistically enhance MO removal from water by the $Er^{3+}$:$YFeO_3$/$TiO_2$-SAC composite. The photocatalytic reaction followed Langmuir–Hinshelwood kinetic model. The $Er^{3+}$:$YFeO_3$/$TiO_2$ particles deposited on SAC could resist a shear force of up to $25 \times 10^{-3}$ N/g without significant dislodgement. The reduced photocatalytic activity of $Er^{3+}$:$YFeO_3$/$TiO_2$-SAC could be attributed to accumulation of MO or its degradation by-products on the surface of the composite rather than photocatalyst poisoning. The calcination treatment would be an effective regeneration technique for the fouled composite.

## Acknowledgements

The authors greatly acknowledge the National Nature Science Foundation of China (50908096, 50908097) and China Postdoctoral Science Foundation (20100471251) for financial supports.

## Appendix A. Calculation for shear force on photocatalyst

Assuming that the solid particles are completely soaked and immersed in suspension, and the friction occurs only between the solid phase and liquid phase, under the same hydraulic condition, the value of friction factor $f_c$ equals the friction factor $f_{l-s}$ in a fluid–solid system, and is calculated by Ergun equation [25]. The shear force on each gram spherical activated carbon (N/g) used in Fig. 8 of the main text was obtained from Chern et al. [24] and is given by

$$f_r = 4f_c\left(\frac{1}{De}\right)\left[\frac{1}{2}\rho_l\left(\frac{U_{lr}}{(1-\alpha)\varepsilon_{lr}}\right)^2\right] \quad (A.1)$$

$$f_{l-s} = 0.583 + \frac{33.3}{Re_l} \quad (A.2)$$

$$De = \frac{2(1-\varepsilon_{sr})}{3\varepsilon_{sr}}\left[1-\sqrt{\alpha}\right]\phi d_p \quad (A.3)$$

$$U_{lr} = \frac{Re_l \mu_l \varepsilon_{lr}}{De\rho_l} \quad (A.4)$$

$$Re_l = \frac{\omega r^2}{2\nu} \quad (A.5)$$

where $f_c$ is friction factor, $De$ is the effective diameter of liquid flow (mm), $U_{lr}$ is the liquid circulation velocity (cm/s), $\varepsilon_{lr}$ is liquid volume fraction, $\rho_l$ is the liquid density (0.9982 g/cm$^3$), $\alpha$ is the gas–fluid volume ratio, and equals to $\varepsilon_{gr}/(\varepsilon_{gr}+\varepsilon_{lr})$, in which $\varepsilon_{gr}$ is the gas volume fraction, $\phi$ is the particle sphericity, $d_p$ is the particle size in diameter (0.6 mm), $Re_l$ is the liquid Reynolds number, $\mu_l$ is the liquid dynamic viscosity (1.0050 mg/cm s), $\nu$ is the liquid kinematic viscosity (0.01 cm$^2$ s), $\omega$ is the liquid angular velocity (rad/s), and $r$ is the rotating liquid flow radius (mm).

## References


[1] T. Robinson, G. McMullan, R. Marchant, P. Nigam, Remediation of dyes in textile effluent: a critical review on current treatment technologies with a proposed alternative, Bioresour. Technol. 77 (2001) 247–255.

[2] A. Fujishima, K. Honda, Electrochemical photolysis of water at a semiconductor electrode, Nature 238 (1972) 37–38.

[3] M.N. Chong, B. Jin, C.W.K. Chow, C. Saint, Recent developments in photocatalytic water treatment technology: a review, Water Res. 44 (2010) 2997–3027.

[4] M.R. Hoffmann, S.T. Martin, W. Choi, D.W. Bahnemann, Environmental applications of semiconductor photocatalysis, Chem. Rev. 95 (1995) 69–96.

[5] D. Dvoranova, V. Brezova, M. Mazur, M.A. Malati, Investigations of metal-doped titanium dioxide photocatalysts, Appl. Catal. B: Environ. 37 (2002) 91–105.

[6] M. Iwasaki, M. Hara, H. Kawada, H. Tada, S. Ito, Cobalt ion-doped $TiO_2$ photocatalyst response to visible light, J. Colloid Interface Sci. 224 (2000) 202–204.

[7] J. Wang, R.H. Li, Z.H. Zhang, W. Sun, R. Xu, Y.P. Xie, Z.Q. Xing, X.D. Zhang, Efficient photocatalytic degradation of organic dyes over titanium dioxide coating upconversion luminescence agent under visible and sunlight irradiation, Appl. Catal. A: Gen. 334 (2008) 227–233.

[8] N.N. Zu, H.G. Yang, Z.W. Dai, Different processes responsible for blue pumped, ultraviolet and violet luminescence in high-concentrated $Er^{3+}$:YAG and low-concentrated $Er^{3+}$:YAP crystals, Phys. B 403 (2008) 174–177.

[9] H.G. Yang, Z.W. Dai, Z.W. Sun, Upconversion luminescence and kinetics in $Er^{3+}$:$YAlO_3$ under 652.2 nm excitation, J. Lumin. 124 (2007) 207–212.

[10] J. Wang, Y.P. Xie, Z.H. Zhang, J. Li, X. Chen, L.Q. Zhang, R. Xu, X.D. Zhang, Photocatalytic degradation of organic dyes with $Er^{3+}$:$YAlO_3$/ZnO composite under solar light, Sol. Energy Mater. Sol. Cell 93 (2009) 355–361.

[11] K. Melghit, O.S. Al-Shukeili, I. Ai-Amri, Effect of M-doping (M = Fe, V) on the photocatalytic activity of nanorod rutile $TiO_2$ for Congo red degradation under the sunlight, Ceram. Int. 35 (2009) 433–439.

[12] N. Grisdanurak, K. Wantala, D. Tipayarom, L. Laokiat, Sonophotocatalytic activity of methyl orange over Fe(III)/$TiO_2$, React. Kinet. Catal. Lett. 97 (2009) 249–254.

[13] T. Torimoto, S. Ito, S. Kuwabata, H. Yoneyama, Effects of adsorbents used as supports for titanium dioxide loading on photocatalytic degradation of propyzamide, Environ. Sci. Technol. 30 (1996) 1275–1281.

[14] T. Tsumura, N. Kojitani, H. Umemura, M. Toyoda, M. Inagaki, Composites between photoactive anatase-type $TiO_2$ and adsorptive carbon, Appl. Surf. Sci. 196 (2002) 429–436.

[15] T.T. Lim, P.S. Yap, M. Srinivasan, A.G. Fane, $TiO_2$/AC composites for synergistic adsorption-photocatalysis processes: present challenges and further developments for water treatment and reclamation, Crit. Rev. Environ. Sci. Technol 41 (2011) 1173–1230.

[16] G.L. Puma, A. Bono, D. Krishnaiah, J.G. Collin, Preparation of titanium dioxide photocatalyst loaded onto activated carbon support using chemical vapor deposition: a review paper, J. Hazard. Mater. 157 (2008) 209–219.

[17] R. Maiti, S. Basu, D. Chakravorty, Synthesis of nanocrystalline $YFeO_3$ and its magnetic properties, J. Magn. Magn. Mater. 321 (2009) 3274–3277.

[18] L.J. Wang, Y.P. Wang, P.Y. Peng, Photocatalytic degradation of L-acid by $TiO_2$ supported on the activated carbon, J. Environ. Sci. China 18 (2006) 562–566.

[19] R.A. Spurr, H. Myers, Quantitative analysis of anatase-rutile mixtures with an X-ray diffractometer, Anal. Chem. 29 (1957) 760–762.

[20] K. Demeestere, J. Dewulf, T. Ohno, P.H. Salgado, H. Van Langenhove, Visible light mediated photocatalytic degradation of gaseous trichloroethylene and dimethyl sulfide on modified titanium dioxide, Appl. Catal. B: Environ. 61 (2005) 140–149.

[21] P.S. Yap, T.T. Lim, Effect of aqueous matrix species on synergistic removal of bisphenol-A under solar irradiation using nitrogen-doped $TiO_2$/AC composite, Appl. Catal. B: Environ. 101 (2011) 709–717.

[22] A. Sclafani, J.M. Herrmann, Comparison of the photoelectronic and photocatalytic activities of various anatase and rutile forms of titania in pure liquid organic phases and in aqueous solutions, J. Phys. Chem. 100 (1996) 13655–13661.

[23] R.I. Bickley, T. Gonzalezcarreno, J.S. Lees, L. Palmisano, R.J.D. Tilley, A structural investigation of titanium-dioxide photocatalysts, J. Solid State Chem. 92 (1991) 178–190.

[24] S.H. Chern, K. Muroyama, L.S. Fan, Hydrodynamics of constrained inverse fluidization and semifluidization in a gas–liquid–solid system, Chem. Eng. Sci. 38 (1983) 1167–1174.

[25] S. Ergun, Fluid flow through packed columns, Chem. Eng. Prog. 48 (1952) 89–94.